

Hemodynamic Monitoring via Model-Based Extended Kalman Filtering: Hemorrhage Resuscitation and Sedation Case Study

Weidi Yin, Ali Tivay, and Jin-Oh Hahn, Senior Member, IEEE

Abstract— This paper investigates the potential of extended Kalman filtering (EKF) for model-based hemodynamic monitoring in a hemorrhage resuscitationsedation case study. To the best of our knowledge, it may be the first model-based state estimation study conducted in the context of hemodynamic monitoring. Built upon a grey-box mathematical model with parametric uncertainty as process noise, the EKF can estimate cardiac output (CO) and total peripheral resistance (TPR) continuously from mean arterial pressure (AP) measurements against interindividual physiological and pharmacological variability. Its unique practical strengths include: it does not require AP waveform as in existing AP-based pulse-contour CO (PCCO) monitors; and it can estimate CO and TPR with explicit account for the effect of sedative drugs. efficacy of the EKF-based hemodynamic monitoring was evaluated based on a large number of plausible virtual patients generated using a collective inference algorithm, which demonstrated that it has significant advantage over open-loop pure prediction, and that its accuracy is comparable to PCCO.

Index Terms— Extended Kalman Filtering, Hemorrhage, Sedation, Hemodynamic Monitoring, Virtual Patient

I. INTRODUCTION

otivated by the recent findings that critical care treatments may be automated to assist clinicians with patient monitoring and titration tasks [1], [2], there is an ever-increasing interest in the development of closed-loop control systems to enable critical care automation, in the areas of fluid resuscitation [3], vasopressor therapy [2], [4], anesthesia and analgesia [5], [6], and mechanical ventilation [7], [8] to list a few.

Each treatment given to a patient induces multiple changes in the patient's physiological state (including, of course, the intended change), some of which are not desired. However, most prior work on closed-loop automation of critical care therapy has focused on the intended treatment endpoint while neglecting other aspects of patient responses, raising concerns related to the safety of closed-loop automation. The situation becomes even more convoluted when multiple closed-loop controlled treatments are to be given to a patient. For example, our prior work demonstrated that hemorrhage resuscitation and intravenous (IV) sedation can interfere with each other in a conflicting manner, possibly driving a patient to a dangerous physiological state [9]: (i) hemorrhage resuscitation to achieve an arterial pressure (AP) target dilutes the sedative drug in the blood and weakens its intended effect, while (ii) IV sedative interrupts hemorrhage resuscitation by lowering AP. For these reasons, although closed-loop controlled treatments appear to successfully drive a patient to desired AP and sedation targets, the patient's internal hemodynamics represented by cardiac output (CO) and total peripheral resistance (TPR) can often be driven to an unacceptably dangerous state [9]. However, CO and TPR cannot be readily measured in clinical practice. Such a limitation presents opportunities related to online estimation of hemodynamics in a patient receiving critical care therapy.

This paper examines the potential of model-based extended Kalman filtering (EKF) for hemodynamic monitoring in a hemorrhage resuscitation-sedation case study. To the best of our knowledge, it is the first model-based state estimation study conducted in the context of hemodynamic monitoring. Built upon a grey-box mathematical model with parametric uncertainty as process noise, the EKF can estimate CO and TPR continuously from mean AP measurements against interindividual physiological and pharmacological variability. Its unique practical strengths include: (i) it does not require AP waveform as in existing AP-based pulse-contour CO (PCCO) monitors and (ii) it can estimate CO and TPR with explicit account for the effect of sedative drugs. The evaluation of the EKF-based hemodynamic monitoring using a large number of plausible virtual patients generated using a collective inference algorithm demonstrated that (i) it has significant advantage over open-loop pure prediction, and that (ii) its accuracy is comparable to PCCO.

II. METHODS

A. Mathematical Model

We used a mathematical model to replicate the combined physiological effects of hemorrhage resuscitation and IV sedation developed in a prior work [9] (Fig. 1). In brief, the mathematical model is composed of (i) blood volume (BV) kinetics in the arterial and venous circulations, (ii) capillarytissue fluid exchange, (iii) autonomic regulation of CO, TPR, and unstressed venous BV, and (iv) sedative pharmacology.

This work was supported in part by the U.S. Office of Naval Research (N00014-19-1-2402) and the U.S. National Science Foundation CAREER Award (CNS-1748762). (Corresponding author: J.-O. Hahn).

W. Yin, A. Tivay, and J.O. Hahn are with the Department of Mechanical Engineering, University of Maryland, College Park, MD 20742, USA (e-mail: wyin12@umd.edu, tivay@umd.edu, jhahn12@umd.edu).

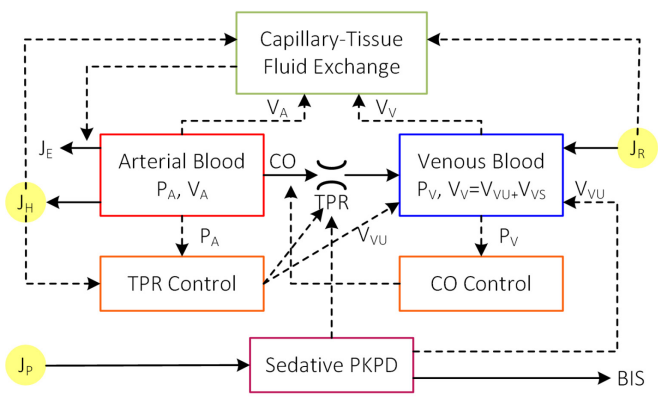


Fig. 1. A mathematical model to replicate the combined physiological effects of hemorrhage resuscitation and intravenous (IV) sedation.

First, BV kinetics represents the changes in arterial and venous BV as well as BP in response to blood loss and fluid gain:

$$\dot{V}_A(t) = Q(t) - [P_A(t) - P_V(t)]/R(t) - J_H(t) - J_E(t)$$
 (1)

$$\dot{V}_V(t) = -Q(t) + [P_A(t) - P_V(t)]/R(t) + J_R(t)$$
 (2)

$$\dot{V}_{RBC}(t) = -J_H(t)V_{RBC}(t)[V_A(t) + V_V(t)]$$
(3)

where V_A , V_V , and V_{RBC} are arterial and venous BV (including plasma and red blood cell (RBC) volumes) as well as RBC volume, Q is CO, R is TPR, P_A and P_V are arterial and venous BP, and J_H , J_R , and J_E are the rates of blood loss, fluid gain, and capillary-tissue fluid exchange rate. P_A and P_V relate to V_A and V_V by arterial and venous capacitances:

$$P_A(t) - P_{A0} = (V_A(t) - V_{A0})/C_A \tag{4}$$

$$P_V(t) - P_{V0} = (V_V(t) - V_{V0} - (V_{VU}(t) - V_{VU0}))/C_V$$
 (5)

where P_{A0} and P_{V0} are nominal arterial and venous BP, V_{VII} is unstressed venous BV, V_{A0} , V_{V0} , V_{VU0} are nominal arterial, venous, and unstressed venous BV, and C_A and C_V are arterial and venous capacitances. Total BV, V, is given by the sum of V_A and V_V :

$$V(t) = V_A(t) + V_V(t) \tag{6}$$

Second, capillary-tissue fluid exchange is modeled phenomenologically to replicate the combined capillary filtration-lymphatic return responses to the change in BV, so that a pre-set fraction of fluid loss and gain leads to the change in BV while the remaining fraction induces the change in the fluid volume in the tissues. Denoting $r_{\rm R}(t)$ the pre-set change in BV in the steady state in response to J_H and J_R:

$$r_B(t) = \frac{1}{1+\alpha_R} \int_0^t J_R(\tau) d\tau - \frac{1}{1+\alpha_H} \int_0^t J_H(\tau) d\tau \tag{7}$$

where α_R and α_H denote the ratio between the changes in BV and tissue fluid volumes in the steady state resulting from cumulative fluid gain and blood loss. The capillary-tissue fluid exchange is modeled as a proportional compensation:

$$J_E = K_E (V(t) - V_0 - r_B(t))$$
 (8)

where V_0 is nominal BV, and K_E is a gain constant. Third, autonomic regulation to maintain BP are phenomenologically modeled so that (i) CO cancels the perturbation in venous BP (i.e., preload); (ii) TPR counteract the change in AP and also reacts to the change in blood viscosity; and (iii) unstressed venous BV counteracts the change in AP. In the Laplace

$$\Delta Q(s) = K_C \frac{s + z_C}{s + p_C} \Delta P_V(s) \tag{9}$$

$$\Delta R(s) = -K_R \frac{1}{s + p_R} \Delta P_A(s) + K_H \Delta H(s) - G_R C_e(s)$$

$$\Delta V_{VU}(s) = -K_{VU} \frac{1}{s + p_R} \Delta P_A(s) + G_{VU} C_e(s)$$
(10)

$$\Delta V_{VU}(s) = -K_{VU} \frac{1}{s + p_R} \Delta P_A(s) + G_{VU} C_e(s)$$
 (11)

where $\Delta Q(t) = Q(t) - Q_0$, $\Delta R(t) = R(t) - R_0$, $\Delta P_A(t) =$ $P_A(t) - P_{A0}$, $\Delta P_V(t) = P_V(t) - P_{V0}$ with Q_0 and R_0 being nominal CO and TPR, $\Delta H(t) = H(t) - H_0$ where H(t) is blood hematocrit defined as $H(t) = \frac{V_{RBC}(t)}{V_A(t) + V_V(t)}$ and H_0 is its nominal value, K_C , K_R , K_H , and K_{VU} are gain constants, p_C and z_C are the pole and zero related to the CO dynamics, p_R is the pole related to the vasomotor tone dynamics, and G_R and G_{VU} are gains related to vasodilation and venodilation effects of the sedative drug. Fourth, the pharmacology of the sedative drug is modeled as a 3-compartment drug mixing model (12)-(14), a 1st-order effect site delay model (15), and drug effect models (10)-(11) and (16) associated with the IV propofol:

$$\dot{m}_1(t) = -(k_{10} + k_{12} + k_{13})m_1(t) + k_{21}m_2(t) +$$

$$k_{31}m_3(t) + J_P(t) (12)$$

$$\dot{m}_2(t) = k_{12}m_1(t) - k_{21}m_2(t) \tag{13}$$

$$\dot{m}_3(t) = k_{13}m_1(t) - k_{31}m_3(t) \tag{14}$$

$$\dot{C}_e(t) = -k_{e0}C_e(t) + \frac{V_P k_{e0} m_1(t)}{V_D(V_A(t) + V_V(t) - V_{RBC}(t))}$$
(15)

$$BIS(t) = F_{BIS}(C_e(t)) \tag{16}$$

where m_1 , m_2 , and m_3 are mass in the central, fast peripheral, and slow peripheral compartments, k_{10} , k_{12} , k_{13} , k_{21} , and k_{31} are rate constants, J_P is propofol administration rate, C_e is sedative concentration at the effect site, k_{e0} is effect site time constant, V_D and V_P are nominal central distribution and plasma volumes, and $F_{BIS}(\cdot)$ is a sigmoidal function relating C_e to BIS, a widely used sedation measure [10]. Note that the mathematical model in Fig. 1 was extensively validated with multiple unpresented datasets, which demonstrated its ability to produce physiologically plausible hemodynamic responses to hemorrhage resuscitation and IV sedation [9].

B. Generation of Virtual Patients

Using the above mathematical model, we derived a virtual patient (VP) generator in the form of probabilistic distributions defined over the model parameters. No experimental data containing the collective hemodynamic responses in a species to simultaneous hemorrhage resuscitation and IV sedation was available. Hence, the VP generator was derived sequentially by (i) deriving a physiological VP generator for (1)-(11) using a dataset, then (ii) deriving a pharmacological VP generator for (10)-(11) using another dataset by leveraging the derived physiological VP generator.

We derived a VP generator for the physiology component (1)-(11) using a collective variational inference (C-VI) algorithm we developed [11] and data collected from 5 sheep undergoing hemorrhage and colloid resuscitation [12]. We structurized the hierarchical relationship between a cohort and subjects therein into a VP generator in the form of the probabilistic graphical model (PGM) in Fig. 2. This PGM represents the dependence between the latent parameters that specify the VP generator (ϕ) , subject-specific characteristics $(\theta_i$'s), and sensor noise $(n_{ij}$'s) pertaining to the mathematical

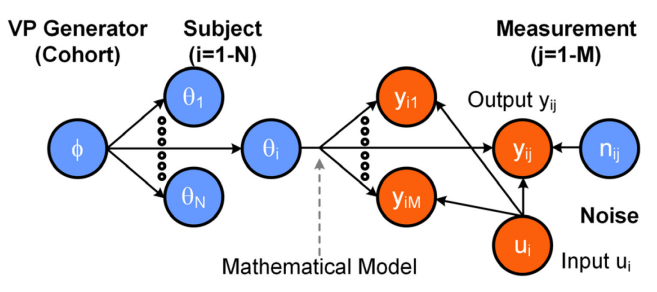


Fig. 2. A probabilistic graphical model that structurizes the hierarchical relationship between a cohort and subjects therein into a VP generator.

model and the output signals created by the VP in response to inputs given to the VP. ϕ denotes the beliefs on the cohort-level model parameters, while θ_i denotes the beliefs on the model parameters associated with subject i (both in the form of diagonal Gaussian densities). y_{ij} is the output signal j in subject i, which can be computed by giving the input signal u_i to the mathematical model in II.A parameterized with θ_i . n_{ij} denotes the SD of the Gaussian noise corrupting y_{ij} .

Then, we estimated the latent parameters in the PGM using the experimental data in [12]. Note that estimating the latent parameters from given data reduces to inferring the following exact yet intractable posterior density:

$$p(\phi, \theta, n|u, y) = p(\phi, \theta, n, u, y)/p(u, y)$$
 (17)
where $p(\phi, \theta, n, u, y) = p(\phi)p(\theta|\phi)p(y|\theta, n, u)p(n)p(u)$
and θ , n , u , and y denote the collections of all the latent
parameters θ_i 's and n_{ij} 's as well as the data u_i 's and y_{ij} 's.
Using modern variational inference methods [13], [14], we
specified an approximate posterior density $q(\phi, \theta, n|v)$ and
inferred it by minimizing the K-L divergence $D_{KL}(v)$ between
 p in (17) and q with respect to the variational parameters v
(which specifies mean and SD of the elements in q expressed
by a family of diagonal Gaussian densities):

 $D_{KL}(\boldsymbol{v}) = \mathbb{E}_q[\log q(\boldsymbol{\phi}, \boldsymbol{\theta}, \boldsymbol{n}|\boldsymbol{v}) - \log p(\boldsymbol{\phi}, \boldsymbol{\theta}, \boldsymbol{n}|\boldsymbol{u}, \boldsymbol{y})]$ (18) We derived an evidence lower bound (19) by substituting (17) into (18), and estimated \boldsymbol{v} by maximizing (19) with stochastic optimization algorithms [15], [16]:

 $L(\boldsymbol{v}) = \log p(\boldsymbol{y}) - D_{KL}(\boldsymbol{v}) = \mathbb{E}_q[\log p(\boldsymbol{y}|\boldsymbol{\theta},\boldsymbol{n},\boldsymbol{u}) + \log p(\boldsymbol{\theta}|\boldsymbol{\phi}) + \log p(\boldsymbol{n}) + \log p(\boldsymbol{\phi}) - \log q(\boldsymbol{\phi},\boldsymbol{\theta},\boldsymbol{n}|\boldsymbol{v})]$ (19) Then, we derived the physiological VP generator in the form of the probability distributions associated with the cohort-level model parameters based on $\boldsymbol{\phi}$ obtained from \boldsymbol{v} .

We derived a VP generator related to the pharmacological effect of IV sedative on vasodilation and venodilation (G_R and G_{VU} in (10)-(11)) using the above physiological VP generator and an extensively validated VP generator for the IV sedative pharmacology applicable to (12)-(16) [17]. We defined a VP generator given by a family of diagonal Gaussian densities associated with G_R and G_{VU} , with mean and SDs as latent parameters. Then, we estimated the latent parameters using the experimental data in [18], by minimizing the discrepancy between the mean and SD associated with mean AP, CO, and TPR responses to IV sedative in [18] versus those predicted by the mathematical model in II.A characterized by a large number of model parameters sampled from the VP generator (including

physiological ϕ , sedative pharmacological in [17], and G_R and G_{VII}).

By construction, the VP generator derived here can provide model parameter samples (i.e., VPs) that can replicate a wide range of variability in hemodynamic behaviors as observed in the data. We used the VP generator in developing the EKFbased hemodynamic monitoring and evaluating it in silico.

C. Extended Kalman Filter Design

We reformulated the mathematical model presented in II.A to a state space representation by defining a state vector $x \triangleq \{x_1, \dots, x_{10}\}$, where $x_1 = \Delta V_A$, $x_2 = \Delta V_V$, $x_3 = \Delta V_{VU}$, $x_4 = s_Q = \Delta Q - K_C \Delta P_V$, $x_5 = \Delta R$, $x_6 = r_B$, $x_7 = \Delta C_e$, $x_8 = \Delta m_1$, $x_9 = \Delta m_2$, and $x_{10} = \Delta m_3$, where all the deviations (i.e., Δs in x) are defined with respect to an initial state (i.e., when the EKF is recruited):

$$\dot{x}(t) = f(\dot{x}(t), u(t), \theta) + w(t)$$

$$y(t_k) = \begin{bmatrix} P_A(t_k) \\ BIS(t_k) \end{bmatrix} = h(\dot{x}(t_k)) + v(t_k)$$
(20)

where θ is the vector of model parameters, w and v are the process and sensor noises, and t_k is a measurement time instant. Noting that the most prominent source of process noise is the parametric uncertainty, we defined w(t) and its covariance matrix as follows [19]:

$$w(t) = J_{\theta}(t)\Delta\theta(t)$$
, $Q_w(t) = J_{\theta}(t)Q_{\theta}J_{\theta}^T(t)$ (21) where $J_{\theta}(t)$ is the Jacobian of $f(x, u, \theta)$ with respect to θ , and $Q_w(t)$ and Q_{θ} are the covariance matrices associated with $w(t)$ and θ , respectively. Note that Q_{θ} is available from the VP generator described in II.B. On the other hand, noting that y consists of direct measurements, we attributed $v(t_k)$ to sensor noise with its covariance matrix Q_R expressed by a diagonal matrix having the noise variances associated with $P_A(t)$ and $BIS(t)$ as its elements.

We constructed the EKF based on (20)-(21) as well as the mean (to define the nominal plant) and SD (to define Q_{θ} , the parametric covariance) of the model parameter values given by the VP generator in II.B. Then, we derived nominal CO and TPR estimates and their confidence intervals using the EKF via its recursive prediction and update procedure. In the prediction step between measurement time instants, the EKF solved (20) and its associated covariance equation to predict the propagation of state and its covariance:

$$\hat{x}^{-}(t_{k}) = \hat{x}(t_{k-1}) + \int_{t_{k-1}}^{t_{k}} f(\hat{x}(t), u(t), \theta) dt$$

$$P^{-}(t_{k}) = P(t_{k-1}) + \int_{t_{k-1}}^{t_{k}} F(t) P(t) + P(t) F^{T}(t) + Q_{w}(t) dt$$

(22)

which was solved via numerical integration, where $F(t) = \frac{\partial f}{\partial x}\Big|_{\hat{x}(t),u(t),\theta}$. In the update step at measurement time instants, the EVE corrected the state estimate and its covariance using

the EKF corrected the state estimate and its covariance using the measurements:

$$K(t_k) = P^{-}(t_k)H^{T}(t_k)[H(t_k)P^{-}(t_k)H^{T}(t_k) + Q_R]^{-1}$$

$$\hat{x}(t_k) = \hat{x}^{-}(t_k) + K(t_k)[y(t_k) - h(\hat{x}^{-}(t_k))]$$
(23)

$$P(t_k) = [I - K(t_k)H(t_k)]P^{-}(t_k)$$
(24)

where $H(t) = \frac{\partial h}{\partial x}\Big|_{\hat{x}(t),\theta}$, and $\hat{x}^-(t_k)$ and $P^-(t_k)$ are predicted state and its covariance at $t = t_k$ before sensor measurements

TABLE I

CARDIAC OUTPUT (CO) AND TOTAL PERIPHERAL RESISTANCE (TPR) ESTIMATION ACCURACY ASSOCIATED WITH EKF AND PURE PREDICTION. ME: MEAN ERROR. MAE: MEAN ABSOLUTE ERROR. SD: STANDARD DEVIATION. IQR: INTER-QUARTILE RANGE. *: P<0.05 (PAIRED T-TEST). †: P<0.05 (WILCOXON RANK-SUM TEST).

	EKF			Pure Prediction		
	ME	MAE	r	ME	MAE	r
	(Mean±SD)	(Median (IQR))	(Mean±SD)	(Mean±SD)	(Median (IQR))	(Mean±SD)
CO [lpm]	-0.1±0.6*	$0.4 (0.2 \text{-} 0.5)^{\dagger}$	0.98±0.03*	-0.2±1.7	0.6 (0.3-0.9)	0.82±0.04
	$(-1.0\pm9.4\%)^*$	$(5.4\% (2.4\% - 8.3\%))^{\dagger}$		$(-2.0\pm16.0\%)$	(7.2% (4.2%-13.6%))	
TPR [mmHg/lpm]	0.1±1.3*	0.8 (0.4-1.5)	0.99±0.00*	0.6±2.2	1.2 (0.7-2.3)	0.80±0.01
	$(1.4\pm8.2\%)^*$	$(4.9\% (2.7\% - 9.1\%))^{\dagger}$		(8.3±20.0%)	(8.3% (5.5%-17.5%))	

become available. Then, we derived $\Delta Q(t_k)$ and $\Delta R(t_k)$ using (9) and (10) based on the EKF estimates.

D. In Silico Evaluation

The EKF-based hemodynamic monitoring was evaluated in silico using 100 VPs, obtained by sampling many VPs from the VP generator in II.B and removing the VPs associated with unrealistic CO and TPR values according to the ranges of CO (2-7 lpm) and TPR (9-40 mmHg/lpm) observed in several in vivo datasets [12], [20], [21]. To rigorously and comprehensively evaluate the EKF, we applied many diverse colloid and propofol infusion regimens to the VPs to elicit a wide range of hemodynamic trajectories, and evaluated the accuracy of CO and TPR estimation. To determine if the EKF has any advantage over prediction, we compared the EKF with open-loop pure prediction (i.e., with $K(t_k) = 0$ in (23)). We used the mean error (ME: mean of the estimation error time series in a hemodynamic trajectory) and mean absolute error (MAE: mean of the absolute estimation error time series in a hemodynamic trajectory) as the metrics of accuracy, and the r value as the metric of trending ability. Further, we also compared the EKF with existing PCCO monitors using the limit of agreement (LoA) as the metric of accuracy.

III. RESULTS

Fig. 3 shows BP-BIS and CO-TPR spaces encompassed by the 100 VPs. Table I summarizes ME, MAE, and the r value associated with the EKF and open-loop pure prediction in estimating CO and TPR. Fig. 4 presents the cumulative distribution of the MAE associated with CO and TPR pertaining to the EKF and open-loop pure prediction. Fig. 5 shows representative examples of successful (corresponding to the circle in Fig. 4), typical (corresponding to the triangle in Fig. 4), and less successful (corresponding to the square in Fig. 4) estimation of CO and TPR based on the EKF associated with Fig. 6 presents the cumulative a therapeutic regimen. distribution of the MAE associated with the state variables responsible for CO $(x_2, x_3, \text{ and } x_4)$ and TPR (x_5) estimation in (25) pertaining to the EKF. Fig. 7 presents a representative example of true versus EKF-estimated state variables associated Fig. 5(a).

IV. DISCUSSION

Naïve application of closed-loop automation to critical care treatments based on intended endpoints alone can put a patient into an undesired physiological state through multi-faceted physiological changes (especially undesired side effects) in response to the treatments. Hence, closed-loop automation of critical care must be accompanied by the ability to monitor a patient's overall hemodynamics beyond what is available from rudimentary sensor measurements. This paper concerns the development of hemodynamic monitoring capability that can estimate CO and TPR in order to preserve patient safety during closed-loop controlled hemorrhage resuscitation and sedation therapy.

The VPs used in the in silico evaluation encompassed a wide range of AP, BIS, CO, and TPR (Fig. 3), suggesting that the in silico evaluation was rigorous and extensive.

The EKF exhibited significantly superior accuracy to pure prediction in both accuracy and trending ability (Table I). In addition, MAE associated with the EKF was small in most VPs, with only a small number of VPs having large MAE (for example, only 10 out of 100 VPs were associated with CO MAE>1 lpm, in contrast to 34 VPs with the same MAE level in case of pure prediction; Fig. 4). The EKF achieved tight tracking of CO and TPR in many VPs (Fig. 5), which is based on the adequate estimation of all the state variables (Fig. 6 and Fig. 7). In particular, the estimation accuracy associated with all the state variables pertaining to CO $(x_2, x_3, \text{ and } x_4)$ and TPR (x_5) were consistently reasonable in many VPs (Fig. 6): (i) the MAE associated with x_2 and x_3 was <10% in most VPs, while (ii) the MAE associated with x_4 and x_5 was <=15% and <=10%, respectively, for >=80% of VPs. Collectively, the results presented here suggest that the EKF-based CO and TPR estimation with AP measurement feedback has clear advantages in enhancing the accuracy and trending ability of hemodynamic monitoring compared to open-loop pure prediction. To the best of our knowledge, our work is perhaps the first study conducted on hemodynamic monitoring via closed-loop model-based state estimation.

In addition to its superiority to open-loop pure prediction, the EKF-based hemodynamic monitoring appeared to exhibit CO estimation accuracy and trending ability comparable to the existing PCCO monitors. The limit of agreement (LoA) in CO estimation associated with the EKF was -1.3-1.1 lpm (Table I), which was superior to 9 out of 10 PCCO monitors reported in a recent review article that were tested under comparable degree of changes in CO (approximately 5 lpm) [22], as well as the LoA pooled from 37 prior studies in another review article [23]. In addition, the r value associated with the EKF-based CO tracking was higher on the average than the pooled r value associated with the PCCO monitors reported in a recent review article (r=0.71) [22]. On top of its efficacy comparable to the existing PCCO monitors, the EKF-based hemodynamic monitoring has a few unique practical advantages relative to the PCCO monitors. First, it uses only mean AP measurement,

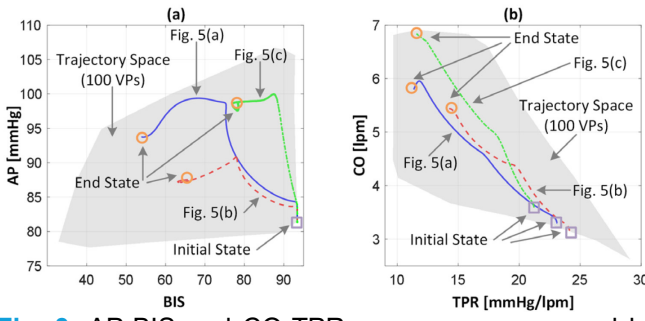


Fig. 3. AP-BIS and CO-TPR spaces encompassed by 100 virtual patients.

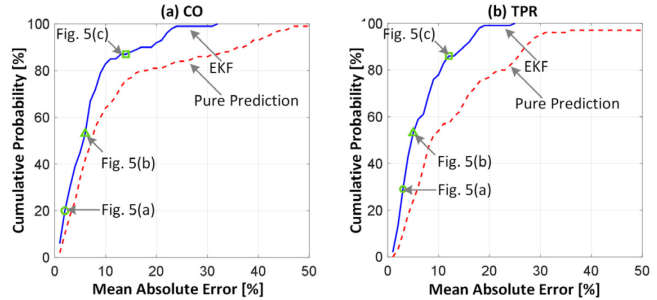


Fig. 4. Cumulative distribution of MAE associated with CO and TPR pertaining to the EKF and open-loop pure prediction.

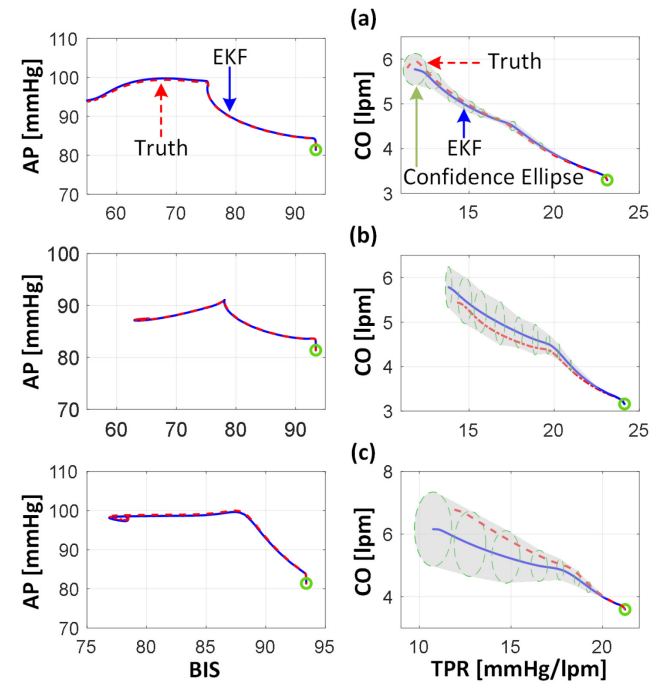


Fig. 5. Representative examples of (a) successful, (b) typical, and (c) less successful estimation of CO and TPR based on the EKF.

which can be ubiquitously acquired using non-invasive blood pressure monitors. In contrast, all the PCCO monitors require the entire AP waveform measurement, which requires invasive arterial catheterization. Second, the EKF-based hemodynamic monitoring allows for CO and TPR estimation with an explicit account for the vasodilation and venodilation effects of IV sedation (via the pharmacological model (12)-(16) embedded in the EKF). In contrast, the PCCO monitors are inherently blinded to the influences of sedative drugs. Considering that

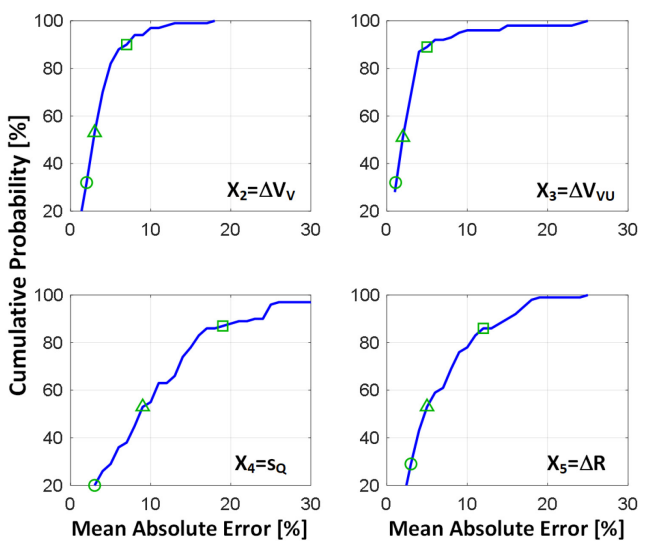


Fig. 6. Cumulative distribution of MAE associated with the state variables responsible for CO (x_2 , x_3 , and x_4) and TPR (x_5) estimation pertaining to the EKF.

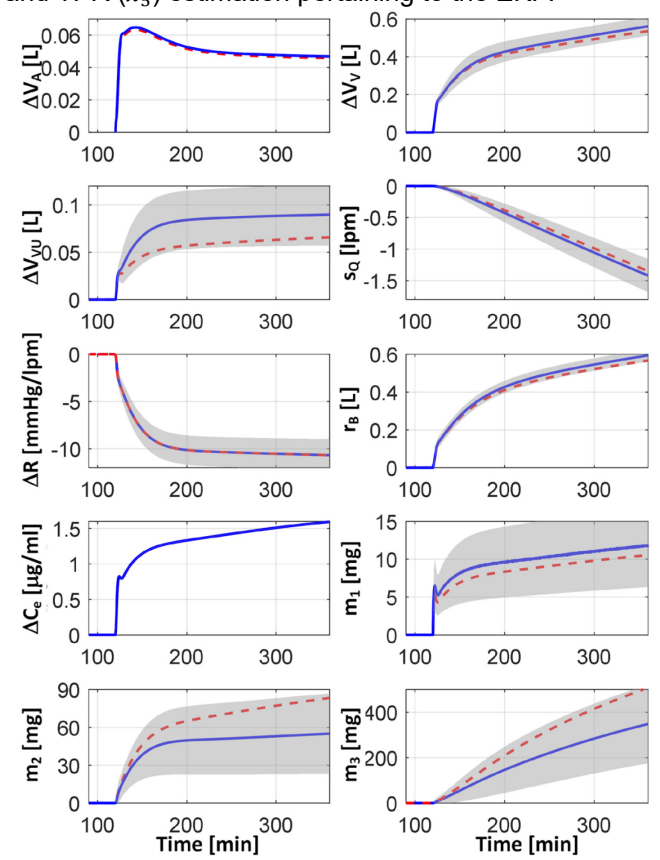


Fig. 7. A representative example of true versus EKF-estimated states. These state estimates correspond to Fig. 5(a). Red dashed lines: true states. Blue solid lines: EKF-estimated states. Grey shades: confidence intervals (±2 standard deviations).

the PCCO monitors tend to suffer from poor accuracy in low TPR states [24], their accuracy may be compromised during the administration of sedative drugs eliciting vasodilation. In sum, the EKF-based hemodynamic monitoring approach has accuracy comparable to the PCCO monitors as well as unique

advantages favorable to its clinical deployment and robustness against diverse physiological state. Hence, model-based state estimation (including the EKF) has the potential to advance hemodynamic monitoring in critically ill patients. Hence, the EKF-based hemodynamic monitoring has the potential to advance hemodynamic monitoring in critically ill patients.

Despite its demonstrated promise and proof-of-concept, this work has a few limitations. First, the VP generator was created using two independent datasets. Feedback control of multiple critical care treatments is an emerging area of research, and an ideal dataset including the effects of simultaneous hemorrhage resuscitation and IV sedation was not available. The sheep data used to build the physiological VP generator had plausible AP, CO, and TPR levels comparable to humans. Hence, the results obtained from this work may be adequate. Regardless, future work must ascertain the efficacy of the EKF using ideal datasets. Second, the evaluation was in silico. The evaluation utilized diverse VPs based on a validated mathematical model. However, mathematical model cannot completely replicate the pathophysiology and pharmacology in critically ill patients as well as the actuator/sensor dynamics and delays. Thus, future work must ascertain the efficacy of the EKF via hardware-inthe-loop simulations as well as in vivo studies. Third, the EKF involves linear approximation of the nonlinear plant dynamics. Despite its promising results, future work to study the potential of nonlinear filtering methods may lead to even more advances in the quality of hemodynamic monitoring.

V. CONCLUSION

This paper illustrated that the EKF may provide a viable solution to hemodynamic monitoring problems during closed-loop controlled hemorrhage resuscitation and IV sedation. Its potential to outperform the state-of-the-art PCCO monitors may foster extensive follow-up research on model-based state estimation approach to hemodynamic monitoring and its use in a broad spectrum of critical care automation challenges, which may all in all revolutionize hemodynamic monitoring to enable holistic tracking of dynamic changes in a patient's physiological state during automated critical care treatments.

REFERENCES

- [1] J. Rinehart, C. Lee, C. Canales, A. Kong, Z. Kain, and M. Cannesson, "Closed-Loop Fluid Administration Compared to Anesthesiologist Management for Hemodynamic Optimization and Resuscitation during Surgery: An In Vivo Study," *Anesthesia and Analgesia*, vol. 117, no. 5, pp. 1119–1129, 2013, doi: 10.1213/ANE.0b013e3182937d61.
- [2] B. L. Sng, H. S. Tan, and a. T. H. Sia, "Closed-Loop Double-Vasopressor Automated System vs Manual Bolus Vasopressor to Treat Hypotension during Spinal Anaesthesia for Caesarean Section: A Randomised Controlled Trial," *Anaesthesia*, vol. 69, pp. 37–45, 2014, doi: 10.1111/anae.12460.
- [3] B. Gholami, W. M. Haddad, J. M. Bailey, and W. W. Muir, "Closed-Loop Control for Fluid Resuscitation: Recent Advances and Future Challenges," Frontiers in Veterinary Science, vol. 8. Frontiers Media S.A., Feb. 23, 2021. doi: 10.3389/fvets.2021.642440.
- [4] A. Joosten et al., "Feasibility of Closed-Loop Titration of Norepinephrine Infusion in Patients Undergoing Moderate- and High-Risk Surgery," British Journal of Anaesthesia, vol. 123, no. 4, pp. 430–438, 2019, doi: 10.1016/j.bja.2019.04.064.
- [5] A. Joosten et al., "Feasibility of Fully Automated Hypnosis, Analgesia, and Fluid Management Using 2 Independent Closed-Loop Systems during Major Vascular Surgery: A Pilot Study," Anesthesia and Analgesia, vol. 128, no. 6, pp. E88–E92, 2019, doi: 10.1213/ANE.0000000000003433.

- [6] G. A. Dumont, "Closed-Loop Control of Anesthesia A Review," in IFAC Proceedings Volumes (IFAC-PapersOnline), 2012, vol. 45, no. 18, pp. 373–378. doi: 10.3182/20120829-3-HU-2029.00102.
- [7] J. Reinders, B. Hunnekens, F. Heck, T. Oomen, and N. van de Wouw, "Adaptive Control for Mechanical Ventilation for Improved Pressure Support," *IEEE Transactions on Control Systems Technology*, vol. 29, no. 1, pp. 180–193, Jan. 2021, doi: 10.1109/TCST.2020.2969381.
- [8] P. von Platen, A. Pomprapa, B. Lachmann, and S. Leonhardt, "The Dawn of Physiological Closed-Loop Ventilation - A Review," *Critical Care*, vol. 24, no. 1. BioMed Central Ltd., Mar. 29, 2020. doi: 10.1186/s13054-020-2810-1.
- [9] W. Yin, A. Tivay, G. C. Kramer, R. Bighamian, and J. O. Hahn, "Conflicting Interactions in Multiple Closed-Loop Controlled Critical Care Treatments: A Hemorrhage Resuscitation-Intravenous Propofol Sedation Case Study," *Biomedical Signal Processing and Control*, vol. 71, Jan. 2022, doi: 10.1016/j.bspc.2021.103268.
- [10] H. Singh, "Bispectral Index (BIS) Monitoring during Propofol-Induced Sedation and Anaesthesia," *European Journal of Anaesthesiology*, vol. 16, no. 1, pp. 31–36, 1999, doi: https://doi.org/10.1046/j.1365-2346.1999.00420.x.
- [11] A. Tivay, G. C. Kramer, and J.-O. Hahn, "Collective Variational Inference for Personalized and Generative Physiological Modeling: A Case Study on Hemorrhage Resuscitation," *IEEE Transactions on Biomedical Engineering*, vol. 69, no. 2, pp. 666–677, 2022, doi: 10.1109/TBME.2021.3103141.
- [12] A. D. Rafie et al., "Hypotensive Resuscitation of Multiple Hemorrhages using Crystalloid and Colloids," Shock, vol. 22, no. 3, pp. 262–269, 2004, doi: 10.1097/01.shk.0000135255.59817.8c.
- [13] D. M. Blei, A. Kucukelbir, and J. D. McAuliffe, "Variational Inference: A Review for Statisticians," J Am Stat Assoc, vol. 112, no. 518, pp. 859–877, 2017.
- [14] D. P. Kingma and M. Welling, "An Introduction to Variational Autoencoders," *Foundations and Trends in Machine Learning*, vol. 12, no. 4, pp. 307–392, 2019, doi: 10.1561/2200000056.
- [15] R. Ranganath, S. Gerrish, and D. M. Blei, "Black Box Variational Inference," *Journal of Machine Learning Research*, vol. 33, pp. 814–822, 2014
- [16] M. D. Hoffman, D. M. Blei, C. Wang, and J. Paisley, "Stochastic Variational Inference," *Journal of Machine Learning Research*, vol. 14, pp. 1303–1347, 2013.
- [17] D. J. Eleveld, P. Colin, A. R. Absalom, and M. M. R. F. Struys, "Pharmacokinetic-Pharmacodynamic Model for Propofol for Broad Application in Anaesthesia and Sedation," *British Journal of Anaesthesia*, vol. 120, no. 5, pp. 942–959, 2018, doi: 10.1016/j.bja.2018.01.018.
- [18] F. de Wit et al., "The Effect of Propofol on Haemodynamics: Cardiac Output, Venous Return, Mean Systemic Filling Pressure, and Vascular Resistances," *British Journal of Anaesthesia*, vol. 116, no. 6, pp. 784–789, 2016, doi: 10.1093/bja/aew126.
- [19] J. Valappil and C. Georgakis, "Systematic Estimation of State Noise Statistics for Extended Kalman Filters," *AIChE Journal*, vol. 46, no. 2, pp. 292–308, 2000, doi: 10.1002/aic.690460209.
- [20] S. U. Vaid et al., "Normotensive and Hypotensive Closed-Loop Resuscitation using 3.0% NaCl to Treat Multiple Hemorrhages in Sheep," Critical Care Medicine, vol. 34, no. 4, pp. 1185–1192, Apr. 2006, doi: 10.1097/01.CCM.0000207341.78696.3A.
- [21] N. R. Marques et al., "Automated Closed-Loop Resuscitation of Multiple Hemorrhages: A Comparison between Fuzzy Logic and Decision Table Controllers in a Sheep Model," Disaster and Military Medicine, vol. 3, p. 1, 2017, doi: 10.1186/s40696-016-0029-0.
- [22] T. Schlöglhofer, H. Gilly, and H. Schima, "Semi-Invasive Measurement of Cardiac Output Based on Pulse Contour: A Review and Analysis," *Canadian Journal of Anesthesia*, vol. 61, no. 5. Springer New York LLC, pp. 452–479, 2014. doi: 10.1007/s12630-014-0135-8.
- [23] A. Joosten et al., "Accuracy and Precision of Non-Invasive Cardiac Output Monitoring Devices in Perioperative Medicine: A Systematic Review and Meta-Analysis," British Journal of Anaesthesia, vol. 118, no. 3. Oxford University Press, pp. 298–310, Mar. 01, 2017. doi: 10.1093/bja/aew461.
- [24] J. Grensemann, "Cardiac Output Monitoring by Pulse Contour Analysis, the Technical Basics of Less-Invasive Techniques," Frontiers in Medicine, vol. 5, no. MAR. Frontiers Media S.A., Mar. 01, 2018. doi: 10.3389/fmed.2018.00064.